On least-cost path for realistic simulation of human motion

A. DATAS, J.Y. FOURQUET and P. CHIRON

Laboratoire Génie de Production, LGP-ENIT, INPT, Université de Toulouse, FRANCE

Abstract

We are interested in "human-like" automatic motion simulation with applications in ergonomics.
The apparent redundancy of the humanoid wrt its explicit tasks leads to the problem of choosing a plausible movement in the framework of redundant kinematics.
Some results have been obtained in the human motion literature for reach motion that involves the position of the hands. We discuss these results and a motion generation scheme associated. When orientation is also explicitly required, very few works are available and even the methods for analysis are not defined.
We discuss the choice for metrics adapted to the orientation, and also the problems encountered in defining a proper metric in both position and orientation. Motion capture and simulations are provided in both cases.
The main goals of this paper are:

- to provide a survey on human motion features at task level for both position and orientation,
- to propose a kinematic control scheme based on these features,
- to define properly the error between motion capture and automatic motion simulation.

Keywords: Motion capture, posture, and motion.

1. Introduction

Human motion generation is highly complex and is concerned with (at least):

- the way the tasks are imposed or characterized
- the way the numerous dof of the human kinematic chain are coordinated for a given task
- how internal dynamics are taken into account
- how interaction with the environment is modeled.

The work described here is devoted to the study of intrinsic properties of the task space and of the mapping at kinematic level between task and joint space. The motivation is not to neglect dynamics - essential in whole-body equilibrium for instance - but to describe a simple framework for plausible human-like motion generation, when dynamics are not decisive. The ideas are tested on sitting reach motions, for both translations and rotations task components.
Generally, the task is denoted by the evolution in space and time of the location X of dimension m. A reaching task consists in reaching a location X^f from X^0. The configuration q of the mechanical system is known when the value of all its n independent joints is known. If $m < n$, the motion problem is under-constrained, sometimes said "ill-posed" in human movement literature, and this setting is known as *kinematic redundancy*. Then, a multiplicity of joint velocities produces the same velocity in task space. The problem can be formulated as an optimization problem in configuration space and, inside this category of problems, minimum-norm solutions leads to weighted pseudo-inversion schemes (Ben-Israel 2003).
Literature on the human movement analysis is mainly focused on reach motion and translation information. Very few works have studied the questions relative to the orientation of the hand or relative to the paths and motions in task space when reaching and grasping is concerned, or when translation and rotation of the end-effector are both imposed.
Questions are numerous: they concern the geometry in task space (shape of paths), significant parameterization (Choe and Faraway 2004; Pierrynowski and Ball 2009), and the temporal aspects (velocity profile), sequences of reach and grasp (Lacquaniti and Soechting 1982; Fan et al. 2006; Hesse and Deubel 2009), simultaneous

*Corresponding author. Email: adrien.datas@enit.fr

evolution of translation and rotation (Wang 1999; Bennis and Brami 2002; ...).
Since coordination of translation and rotation is the focal point, time-scale and length-scale are obviously concerned. As a result of human motion studies, no "fundamental human motion principle" emerges but optimization principles have proved to be useful guides.
In this paper, we focus on seated reaching motions in the horizontal plane and tend to reproduce human motions based on well known Morasso experiments (Morasso 1981). The simulations are realized with a 24 Degrees of Freedom (DOF) virtual human (see Fig. 1).

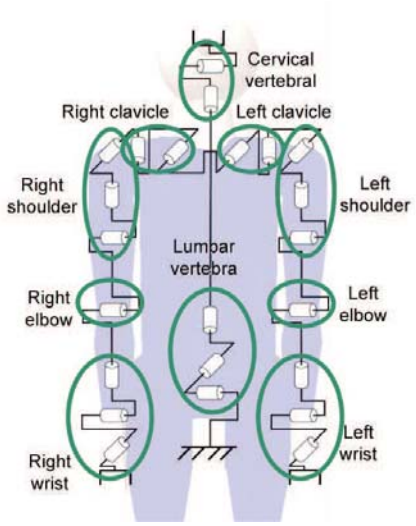

Fig. 1. Virtual human kinematic structure

In the next section, translation paths are studied and a kinematics-based scheme is proposed when task path requires too much joint displacement. Section 3 presents a similar approach for rotations. Finally, the last section discusses the translation and rotation coordination. In every section, motion capture and simulation curves are provided.

2. Translation constraints

2.1. Distance, path and motion in task space

In this case, the location X_p is made of the Cartesian coordinates $X_p = (x, y, z)$ of a specific body (hand, head ...) and the natural way to measure length and distance is to use the Euclidean metric. Various authors have studied the reach motion in free space.
In many cases reported in the literature, the observed path, in particular for planar movement, is close to straight lines (Flash and Hogan 1985; Soechting and Lacquaniti 1981) and the motion along the path exhibits a bell-shaped velocity profile (Morasso 1981; Atkeson and Hollerbach 1985).

This behavior has been associated to integral criteria, first in task-space. Among them, the measures substantiate the *minimum hand jerk* solution (Flash and Hogan 1985) i.e. the solution $X_p(t)$ that minimizes:

$$C = \frac{1}{2}\int_0^{t_f}\left\{\left(\frac{d^3x}{dt^3}\right)^2 + \left(\frac{d^3y}{dt^3}\right)^2 + \left(\frac{d^3z}{dt^3}\right)^2\right\}dt \qquad (1)$$

where t_f is the total duration of the motion and under the constraints that the derivatives $\frac{d^2x}{dt^2}, \frac{d^2y}{dt^2}, \frac{d^2z}{dt^2}, \frac{dx}{dt}, \frac{dy}{dt}, \frac{dz}{dt}$ all equal zero at both endpoints.
In fact, the Calculus of Variations (Gelfand and Fomin 2000) enables us to conclude that since there is no coupling between the Cartesian coordinates, the path solution of (1) is naturally a straight line. If this path $X_p(s)$ is parameterized by its curvilinear abscissa s ($s \in [0,1]$, and $X_p(s=0) = X_p^0$ and $X_p(s=1) = X_p^f$, then the minimum hand jerk impose the following time law along the path:

$$s(t) = a_5t^5 + a_4t^4 + a_3t^3 + a_0, 0 \le t \le t^f \qquad (2)$$

where the coefficients a_i depend on the endpoints value X_p^0 and X_p^f and on t^f.
This solution provides the minimum distance path - the geodesic - in the usual Cartesian metrics covered with a smooth time profile verifying the minimum jerk solution along this straight line.
Thus a way to program human-like simulation for a variety of position tasks is to impose a straight line $X_p(s)$ and the $s(t)$ law defined in relation (2) on this straight line.
In fact, several authors have shown that the reference path is not always a straight path and some of them attempted to define new criteria in order to explain these discrepancies.
On the one hand, one may think that evolution has led to render the human locomotor apparatus really efficient and turn him able to follow the most efficient paths in Cartesian space: the straight line. Remark that statistical methods popularized in industrial cycle-time measurement such as MTM implicitly include this fact since the cycle-time in usual workplaces is only related to distance of reach (Stegemerten et al. 1948; Kuhn and Laurig 1990; Laring et al. 2002; Ma et al. 2010).
On the other hand, we know that kinematic chains are not isotropic motion generators in Cartesian space. Thus, intuitively, one can infer that there is a preferred workspace zone in which the path is a straight line, and other zones in which the mechanical constraints induced by the nature of kinematic chains will render really difficult to follow a straight line.
Here, the matter is not so much to ask if the optimization criterion acts in Cartesian space or in

Joint Space (Engelbrecht 2001; Svinin et al. 2005) but rather how to reproduce a trade-off between the task efficiency and the constraints induced by the mechanical structure.

2.2. Space mappings and mixed criteria

The relation between the respective first order variations δX_p and δq, or the exact relation between the velocities $\dot{X}_p$ and $\dot{q}$, writes as a linear map:

$$\delta X_p = J_p \delta q \text{ or } \dot{X}_p = J_p \dot{q} \quad (3)$$

where $J_p = J_p(q)$ is the $3\times n$ Jacobian matrix associated to the task $\dot{X}_p$.

This mapping is configuration-dependent and does not provide an isotropic transformation from joint space to task space. The properties of this mapping are enlightened by its singular value decomposition (SVD) (Golub and Van Loan 1983). SVD provides the means to analyze the amount of joint displacement necessary to move in a given direction in task space. SVD of J_p writes:

$$J_p = U \Sigma V^T \quad (4)$$

where $U = [u_1 u_2 \dots u_m]$ is an orthonormal basis of the tangent vectors to the task space, $V = [v_1 v_2 \dots v_n]$ is an orthonormal basis of the tangent space to the configuration space, $\Sigma = diag\{\sigma_1, \sigma_2, \dots, \sigma_p\}$ is a $m\times n$ diagonal matrix with rank $p = min\{m, n\}$ and the singular values σ_i of J_p are arranged such that $\sigma_1 \geq \sigma_2 \geq \cdots \geq \sigma_p \geq 0$.

The geometrical meaning of this decomposition is : J_p maps a unit ball in the tangent space to the task space into a p-dimensional ellipsoid in the tangent space to the configuration space. This ellipsoid has principal axes u_i with length σ_i. Remark that the $\{u_i; i = 1, \dots, p \leq m\}$ form a basis for the range of J_p and the $\{v_i; i = p+1, \dots, n\}$ form a basis of the kernel of J_p.

Thus, a significant difference of value among the σ_i implies that the amount of joint displacement consumed for a given norm of task displacement in task space varies with the direction and that some directions in task space are really easier to follow.

Thus, on the one hand, one may think that human motion will occur in straight line if the task path does not require a large amount of joint motion. On the other hand, some configurations are such that task displacement in a certain direction requires a really high amount of joint motion: in this latter case, at least one singular value takes a significant smaller value and straight paths are not necessarily efficient.

2.3. The motion scheme

The proposed approach consists in choosing straight lines as initial guesses for the Cartesian path and to adapt this guess depending on the SVD. Thus, the simulated movements are built upon optimization in path space under the condition of a reasonable expense in joint space.

This program is realized on the basis of a kinematic control scheme where lower singular-values filtering acts when SVD detects that the straight line is too costly at joint level. The control scheme is the following:

$$\delta q = J^{+}_{W,F}\, \delta X_p + P_p z \quad (5)$$

where the main task consists in following the Cartesian path and $P_p z$ is a secondary task built upon :

- the projector P_p into the null space of J_p,
- an n-dimensional vector z computed as the scaled gradient of a potential field that enables to take into account inequality constraints such as joint limit avoidance and reference posture adjustment.

The main task uses the weighted and filtered pseudoinverse of J_p (Ben-Israel and Greville 2003):

$$J^{+}_{W,F} = W^{-1} J^t (J W^{-1} J^t + F)^{-1} \quad (6)$$

where W is the inertia matrix and F stands for the $n\times n$ filtering matrix (Maciejewski 1990) computed by :

$$F = \sum_{i=1}^{n} (\alpha_i^2 u_i u_i^t) \quad (7)$$

In this matrix, the respective weight α_i of the u_i components is directly related to the value of σ_i. A threshold on σ_i value has been computed from captured motions paths (Hue et al. 2008), by computing singular values for straight and curved Cartesian paths. If the singular value σ_i is upper this threshold, then $\alpha_i = 0$ and $J^{+}_{W,F}$ is the inertia-weighted pseudo-inverse of J_p, else α_i takes a non-zero value along a continuous $\alpha_i(\sigma_i)$ profile.

2.4. Motion capture and simulation results

Motion capture is based on a sequence of Morasso (Morasso 1981) of reaching movements on the horizontal plane. This experiment exhibits the fact that the hand follows a straight line for several cases but that a curved path appear for some other cases. The hand velocity matches the bell-shaped profile of minimum hand jerk criterion.

In simulation, the same tuning of our control scheme exhibits similar path features (see Fig. 2) : it produces straight lines motions when it is efficient to follow them and it switches to curved paths when kinematics prescribe a locally better path. Comparison of solutions, captured and

simulated, are made through the usual Cartesian distance measure through the Linearity Index (*LI*) (Wang 1999). The *LI* is a measure of path curvature. The smaller the *LI* is, the straighter the path is.

For the straight line, the motion capture has a $LI = 2.15\%$ and the simulated $LI = 1.12\%$. For the curved lines, motion capture has a mean $LI = 3.68\%$ and the simulated *LI* for this case is equal to 4.027%. The values obtained for these index are significant in both examples.

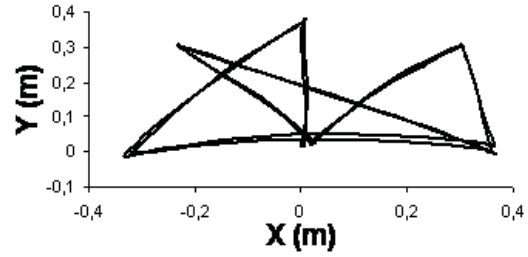

Path of the hand for captured motion

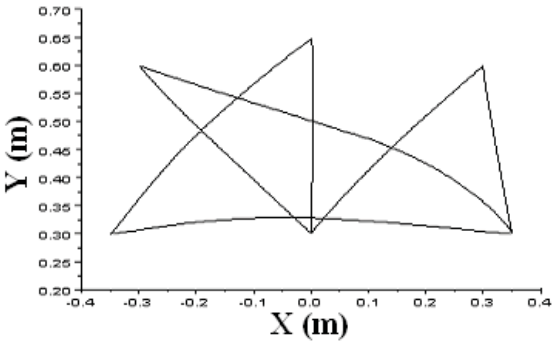

Path of the hand for simulated motion

Fig. 2. Hand translation paths

3. Rotation constraints

Human manipulation tasks (touch, grasp, carry) are such that the position and orientation of the hand(s) is partially or totally known.

If the task presents a symmetry, one rotation can be left free, but in many cases it is desirable to impose the orientation of the hands as the result of the definition of a task.

3.1. Distance, path and motion in task space

Intrinsically, rotations are elements of *SO(3)* (the Special Orthogonal Group of dimension 3), a 3-dimensional differential manifold with a Lie group structure. A point in this manifold is computed in coordinates by several choices, through various parameterizations. Among them, some are made of surabondant not independent components (rotation matrices), some other are endowed with a minimal number of components (3-angles systems: Euler, Bryant, Yaw-Pitch-Roll ...) but also with singularities ("gimbal lock"). Axis-Angle representation, unit quaternion, exponential map are formalisms that are really close to the canonical coordinates of *SO(3)*. Here, the following developments mainly use the exponential map formalism (Park and Ravani 1997; Murray et al. 1994).

We try to follow, as for the translation, the geodesic path in rotation. We first define a least distance path on *SO(3)*, and second interpolate a minimum jerk time-evolution along this path.

Let denote $R = (r_{ij})$ a rotation matrix. Since Euler (Murray et al. 1994), we know that it is possible to transform a rotation matrix (or an orthonormal vector frame) R_0 into a rotation (or another vector frame) R_1 by defining a vector ω around which an amount of rotation $\Theta \in [0,2\pi[$ is performed. The exponential map formalism exploits this axis-angle representation.

Let us denote $[\hat{a}]$ the skew-symmetric 3×3 matrix derived from the $\mathbb{R}^3$ vector a that enables to transform the cross-product in a matrix multiplication $a \times b = [\hat{a}].b$.

Then $\dot{R} = \omega \times R$ writes $\dot{R} = [\hat{\omega}]R$. The solution of this linear matrix differential equation is $R(t) = \exp([\hat{\omega}]t)R(0)$ where 'expm' stands for matrix exponential and is given for $\|\omega\| = 1$ by:

$$\exp([\hat{\omega}]\theta) = \mathrm{I} + [\hat{\omega}]\sin\theta + [\hat{\omega}]^2(1 - \cos\theta) \quad (8)$$

In the same way, it is possible to prove the existence of (ω, Θ) with $\|\omega\| = 1$ and $\Theta \in [0,2\pi[$ such that the motion between two orientations R_0 and R_1 is given by : $R(t) = \exp([\hat{\omega}]t)R(0)$. The geodesic on $SO(3)$ between R_0 and R_1 is obtained by rotating around ω with a Θ amount and the equation (8) provides a natural way to interpolate on the geodesic.

Conversely, one can write $\omega t = \log(R(t)R_0^t)$ where 'logm' stands for the matrix logarithm and is given by : $\log(R) = \frac{\Theta}{2\sin\Theta}(R - R^t)$ with $\Theta = \cos^{-1}\frac{(\mathrm{trace}(R)-1)}{2}$.

Note that ω can be obtained in various ways (from the rotation matrices or quaternion, for instance) and is given by the formula (with $R = R_1R_0^t$) :

$$\omega = \log(R) = \frac{1}{2\sin\Theta}\begin{bmatrix} r_{32} - r_{23} \\ r_{13} - r_{31} \\ r_{21} - r_{12} \end{bmatrix}$$

The distance between two rotations is the length of the shortest path between them. It is then computed along geodesics. In *SO(3)*, this distance d_r between two rotations R_0 and R_1 is given by:

$$d_r(R_0, R_1) = \|log m(R_0^t R_1)\|_{fro}$$

where $\|A\|_{fro} = \mathrm{trace}\left(\sqrt{A^tA}\right) = \sqrt{\Sigma_i \sigma_i^2}$ is the Frobenius norm of the matrix *A*.

Then, if θ varies linearly as a function of the time $\theta(t) = \mu t + \square$, the motion is a linear interpolation from R_0 to R_1 along the geodesic. This simple solution is the one provided by the *slerp* algorithm

(Shoemake 1985) popularized with unit quaternions. It provides a constant velocity evolution on the geodesic. From the physics, such a behavior seems unnatural since it requires infinite acceleration at the beginning and at the end. Remarking that translation and rotation result from the same biomechanical system, it is plausible that the time evolution of the variables obeys the same smoothness properties. Then, again minimizing the jerk along the geodesic is the chosen solution and thus: $\theta(t) = a_5 t^5 + a_4 t^4 + a_3 t^3 + a_0, 0 \leq t \leq t^f$

3.2. space mapping and optimization

Tangent vectors to *SO(3)* are related to joint velocities by the canonical linear map:

$$\omega = \mathrm{J_r}\dot{\mathrm{q}} \qquad (9)$$

where J_r is a 3×3 matrix.
Then, the animation problem requires first that ω and $\Theta(t)$ be given and second to provide a generalized inversion scheme for the linear system (9). Again, the norm of the tangent vectors in both spaces can be efficiently computed by SVD which gives a local measure of preferred directions in task space for a given configuration.

3.3. Motion capture results

The idea is to experiment a simple rotation without translation of the reference point. We ask the subjects to rotate the pose of the hand between two drawn orientations superposed at the same position. The motion capture results are presented in the figures 3 and 4.

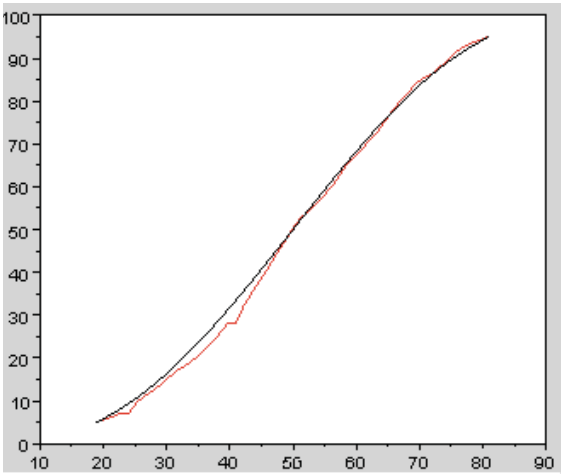

Fig. 3. Experiment 2 : Comparizon between time evolution of captured rotation of the hand (red) and the unidimensional minimum jerk curve (black).

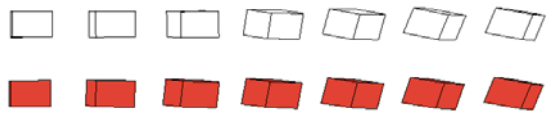

Fig. 4. Experiment 2 : Boxes representative of the time evolution of the rotation. White boxes (top) represent the captured movement. Orange boxes (down) represent the rotation geodesic.

The figure 3 shows that the time profile for a simple movement of rotation around the vertical axis is really similar to the minimum jerk profile.
The figure 4 represents the time evolution of the rotation (from left to right) at regularly spaced instants. Even if the captured motion is slightly different from the geodesic, the motion appears similar and the maximum measured distance is: $d_{r_{max}} = 0.152$.

4. Combining rotations and translations

4.1. Discussion

The task simulation amounts to the definition of the interpolation laws for both the position of a particular point of the hand (the Tool Center Point (TCP)) and the orientation of a body-fixed frame. Such a composite object lives in *SE(3)*, the Special Euclidean group of dimension 3.
The associated differential kinematics writes:

$$\begin{bmatrix} v \\ \omega \end{bmatrix} = \begin{bmatrix} J_p \\ J_r \end{bmatrix} \dot{q} \qquad (10)$$

Different possibilities arise in choosing the solution of this linear system. On one side, one may think that translation and rotation follow their own rule, independently in two parallel spaces, $\mathbb{R}^3$ for the Cartesian coordinates, *SO(3)* for the orientation parameters. Intrinsic metric and closed-form geodesics are available in each space. Following this idea leads to obtain a straight line motion in Cartesian space for the TCP and a geodesic in *SO(3)* for the frame attached to the body. We may think that this independence is dubious. In fact, beyond the fact that this problem is solvable in a well-posed setting with natural metrics, at least two other arguments speak for this solution. Firstly, this decoupling is observed naturally in the motion of bodies : in absence of external forces, the linear and angular velocities keep constant values and the resulting path follows in parallel the geodesics of $\mathbb{R}^3$ and *SO(3)*. Secondly, *SE(3)* is not the cross-product of $\mathbb{R}^3$ and *SO(3)* and there is no natural (i.e. no bi-invariant) metric on it (Zefran and Kumar 1996). Thus, choosing a metric in *SE(3)* requires to weight two mathematical objects of different nature with an unique measure of length. Such a weighting has no intrinsic meaning from the geometric point of view. It amounts to choose a Riemannian metric (Arimoto et al. 2009) on *SE(3)* defined by a block-diagonal matrix *W* related to the length *l* by:

$$\mathrm{W} = \begin{bmatrix} \beta \mathrm{I} & 0 \\ 0 & \delta \mathrm{I} \end{bmatrix} \text{ and } \mathrm{l} = \sqrt{\sum \beta_{ij} v_i v_j + \sum \delta_{ij} \omega_i \omega_j} \qquad (11)$$

This is equivalent to the choice of a length scale between s and θ. This choice may be motivated by different reasons and the synchronization of translations and rotations may be viewed as time or/and length scale.

In some captured motions, we observe paths that are fairly far from the geodesics, for the translation or the rotation part, or for both. This is in particular the case for motion in which the amount of rotation is really important, and should require that the translation does not occur along a straight line.

Thus, again the geometry of the task space is not the sole decisive factor in the generation of human motion. The way rotation and translation constraints interfere in determining a good path in *SE(3)* is not easy to understand. If one applies the filtering scheme illustrated for the translation parameters, it must be kept in mind that the singular values of the global map (10) are dependent on the choice of length made in (11).

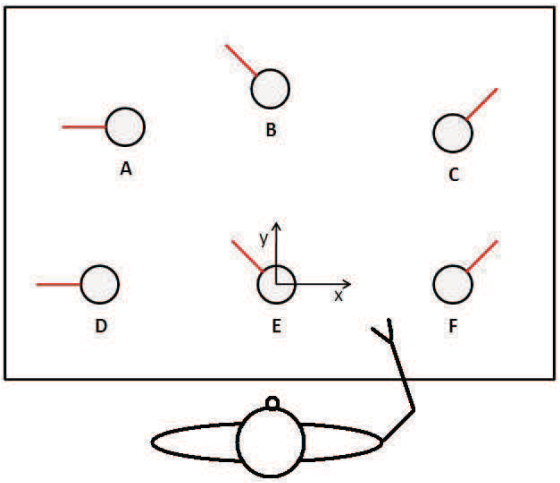

Figure 5: Experiment 3 : position and rotation constraints

4.2. Motion capture and simulation

The experiment of paragraph 2 is modified in the way depicted at figure 5 and tested with 8 subjects. Each subject has to follow the sequence given by (12), and positions and orientation are given in Table 1.

$$E \Rightarrow B \Rightarrow D \Rightarrow F \Rightarrow C \Rightarrow E \Rightarrow A \Rightarrow F \qquad (12)$$

Table 1: Hand positions and orientations

Point	Position X	Position Y	Orientation
A	-25	30	+90°
B	0	25	+45°
C	30	29	-45°
D	-30	0	+90°
E	0	0	+45°
F	30	0	-45°

For illustrating purposes, we focus here on two movements depicted in red in the figures: a first one, from (E) to (A), for which the translation observed is close to a straight line, and a second one, from (D) to (F), for which this translation occurs along a curve really different from a straight line. In both movements, the time and space evolution are studied.

The first movement is represented in figures 6 and 7.

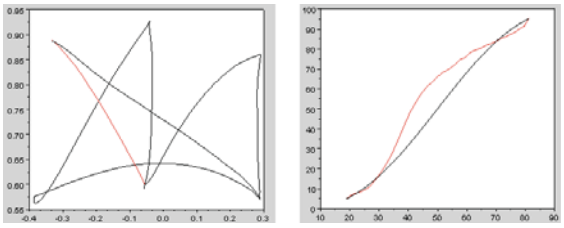

Figure 6: Experiment 3.1 : (a) - translation part of the global sequence of movements (black) and of the studied movement (red) (b) - Comparison between the time evolution of the hand orientation (red) and the minimum jerk (black).

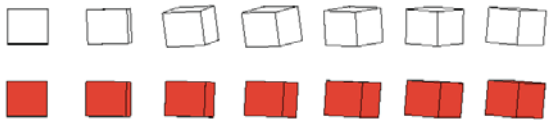

Figure 7: Experiment 3.1 : Boxes representative of the time evolution of the rotation. White boxes (top) represent the **captured** movement. Orange boxes (down) represent the rotation geodesic.

Contrary to the observations for the pure rotation movement, the figure 6 shows that the time profile may be different from the minimum jerk profile. Moreover, the figure 7 shows that the human movement does not always follow the shortest rotation path. The distance between the shortest path and this movement are $LI = 4.16\%$ for the position and $d_{r_{max}} = 0.45$ for the rotation.

The second captured movement is represented in the figures 8 and 9.

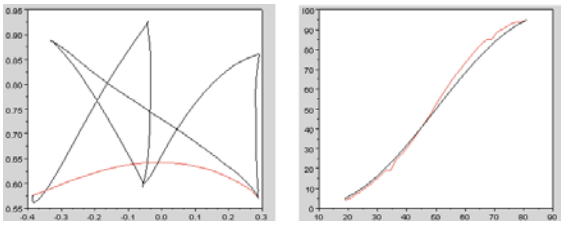

Figure 8: Experiment 3.2 : (a) - translation part of the global sequence of movements (black) and of the studied movement (red) (b) - Comparizon between the time evolution of the hand orientation (red) and the minimum jerk (black).

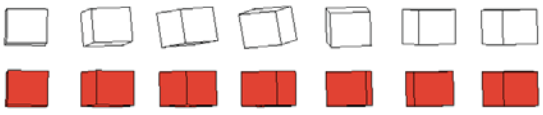

Figure 9: Experiment 3.2 : Boxes representative of the time evolution of the rotation. White boxes (top)

represent the **captured** movement. Orange boxes (down) represent the rotation geodesic.

Here, the rotation time profile is identical to a minimum jerk profile (see Fig. 8) but the rotation does not follow the rotation shortest path (see Fig 9). The differences between the shortest path and the captured movement are $LI = 10.16\%$ for the position and $d_{r_{max}} = 0.35$ for the rotation.
Both movements are simulated with the kinematic control scheme described in the section 2. The reference paths are the geodesics in rotation and translation, and these paths are covered with a minimum jerk profile after a length-scale in order to synchronize rotation and translation components. SVD filtering is applied globally on a translation and rotation task in order to take into account the cost in joint space.
The results of the first movement are given in the figures 10 and 11; the results of the second one are given in the figures 12 and 13.

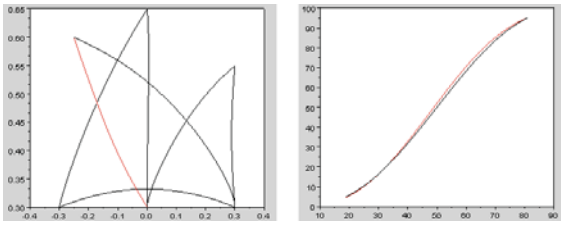

Figure 10: Experiment 3.1 (**simulation**) : (a) - translation part of the global sequence of movements (black) and of the studied movement (red) (b) - Comparizon between the time evolution of the hand orientation (red) and the minimum jerk (black).

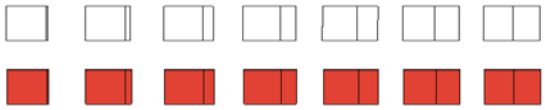

Figure 11: Experiment 3.1 : Boxes representative of the time evolution of the rotation. White boxes (top) represent the **simulated** movement. Orange boxes (down) represent the rotation geodesic.

The simulation of the experiment 3.1 has a deformation about 1.97%. The measured maximum distance for the rotation is: $d_{r_{max}} = 0.027$. For the experiment 3.2, the results are $LI = 5.32\%$ for the position and a distance of $d_{r_{max}} = 0.03$ for the rotation. These simulations are dependent on the tuning of the SVD filtering that amounts to weight rotation and translation on one side, internal kinematic constraints on the other.
It is shown that various features can be conserved (SVD deformation in translation, minimum jerk rotation time profile) but that it is difficult to predict which component is prevalent in a given movement.
Much work remains necessary to analyze which metrics are pertinent and how space and time constraints interact.

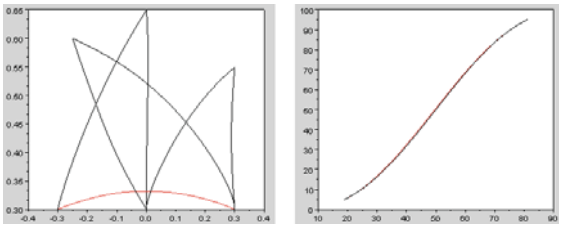

Figure 12: Experiment 3.2 (**simulation**) : (a) - translation part of the global sequence of movements (black) and of the studied movement (red) (b) - Comparizon between the time evolution of the hand orientation (red) and the minimum jerk (black).

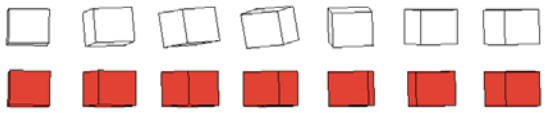

Figure 13: Experiment 3.2 : Boxes representative of the time evolution of the rotation. White boxes (top) represent the simulated movement. Orange boxes (down) represent the rotation geodesic.

5. Conclusion

This work aims at studying the relationships between kinematics, optimization principles and human motion. Metrics and shortest paths have been defined and tested in real and simulation.
Many cases arise and some of the key features that appear in the real movements can be reproduced or predicted by a kinematic control scheme with least-cost principles. Shortest paths in the separate metrics, for rotation and translation, are present but are not the only possible paths. Minimum jerk time profile is also present but is sometimes slower than the observed time profile, and much work remains necessary to analyze how space and time constraints interact. This may prove the need for the definition of coupled metrics in *SE(3)* or for a proper weighting between geometric cost in task space, geometric cost in joint space and internal dynamics constraints. Another approach could be to prioritize translation and rotation tasks in order to filter independently both components of the task.

References

S. Arimoto, M. Yoshida, M.Sekimoto, and K. Tahara. A riemannian geometry approach for control of robotic systems under constraints. SICE Journal of Control, Measurement, and System Integration, 2(2):107–116, 2009.
C.G. Atkeson and J.M. Hollerbach. Kinematic features of unrestrained arm movements. Journal of Neuroscience, 5:2318–2330, 1985.
A. Ben-Israel and T.N.E Greville. Generalized inverse theory. Springer, 2003.

N. Bennis and A.R. Brami. Coupling between reaching movement di- rection and hand orientation for grasping. Brain Research, 952(2):257 – 267, 2002.

S.B. Choe and J.J. Faraway. Modeling head and hand orientation during motion using quaternions. Proceeding of the SAE Digital Human Modeling for Design and Engineering Conference, June 15-17 2004.

S.A. Engelbrecht. Minimum principles in motor control. Journal of Mathematical Psychology, 45:497–542, 2001.

J. Fan, J. He, and S.I. Helms Tillery. Control orientation and arm movement during reach and grasp. Experimental Brain Research, 171(3):283–296, 2006.

T. Flash and N. Hogan. The coordination of arm movements: An ex- perimentally confirmed mathematical model. Journal of Neuroscience, 5(7):1688–1703, 1985.

I.M. Gelfand and S.V. Fomin. Calculus of variations. Dover, 2000.

G.H. Golub and C.F. Van Loan. Matrix computations. John Hopkins studies in Mathematical Sciences, 1983.

C. Hesse and H. Deubel. Changes in grasping kinematics due to different start postures of the hand. Human Movement Science, 28(4):415 – 436, 2009.

V. Hue, J.Y. Fourquet, and P. Chiron. On realistic human motion simulation for virtual manipulation tasks. In 10th International Conference on Control, Automation, Robotics and Vision, pages 167 –172, dec. 2008.

F.M. Kuhn and W. Laurig. Computer-aided workload analysis using MTM. In Computer-aided ergonomics - A researcher s guide. Taylor and Francis, 1990.

F. Lacquaniti and J.F. Soechting. Coordination of arm and wrist motion during a reaching task. The Journal of Neuroscience, 2(4):399–408, 1982.

J. Laring, M. Forsman, R. Kadefors, and R. Ortengren. Mtm-based ergonomic workload analysis. International Journal of Industrial Ergonomics, 30(3):135 – 148, 2002.

L. Ma, W. Zhang, H. Fu, Y. Guo, D. Chablat, and F. Bennis. A framework for interactive work design based on digital work analysis and simulation. Human Factors and Ergonomics in Manufacturing and Service Industries, abs/1006.5226, 2010.

A.A. Maciejewski.Motion simulation: Dealing with the ill- conditioned equations of motion for articulated figures. IEEE Comput. Graph. Appl., 10(3):63–71, 1990.P. Morasso. Spatial control of arm movements. Experimental Brain Research, 42:223–227, 1981.

R.M. Murray, S. Sastry, and L. Zexiang. A Mathematical Introduction to Robotic Manipulation. CRC Press, Inc., Boca Raton, FL, USA, 1994.

F.C. Park and B. Ravani. Smooth invariant interpolation of rotations. ACM Trans. Graph., 16(3):277–295, 1997.

M.R. Pierrynowski and K.A. Ball. Oppugning the assumptions of spatial averaging of segment and joint orientations. Journal of Biomechanics, 42:375–378, 2009.

K. Shoemake. Animating rotation with quaternion curves. SIGGRAPH Comput. Graph., 19(3):245–254, 1985.

J.F. Soechting and F. Lacquaniti. Invariant characteristics of a pointing movement in man. The Journal of Neuroscience, 1(7):710–720, 1981.

G. J. Stegemerten H. B. Maynard and J. L. Schwab. Methods-time measurement. McGraw-Hill industrial organization and management series, N. Y., 1948.

M. Svinin, Y. Masui, Z-W. Luo, and S. Hosoe. On the dynamic version of the minimum hand jerk criterion. J. Robot. Syst., 22:661–676, 2005.

X. Wang. Three-dimensional kinematic analysis of influence of hand orientation and joint limits on the control of arm postures and movements. Biological Cybernetics, 80:449–463, 1999.

M. Zefran and V. Kumar. Planning of smooth motions on se(3). In Proceedings of the 1996 IEEE International Conference on Robotics and Automation, Minneapolis, Minnesota, April 1996.